Multipactor suppression by micro-structured gold/silver coatings for space applications

Valentin Nistor[a,*], Luis A. González[a], Lydya Aguilera[b], Isabel Montero[b], Luis Galán[a], Ulrich Wochner[c], David Raboso[d]

[a] *Departamento de Fisica Aplicada, Universidad Autonoma de Madrid, Cantoblanco, 28049 Madrid, Spain*
[b] *Instituto de Ciencia de Materiales de Madrid (CSIC), Cantoblanco, 28049 Madrid, Spain*
[c] *Tesat Spacecom GmbH & Co. KG,Gerberstr. 49, D-71522 Backnang, Germany*
[d] *European Space Agency (ESA), European Space Research and Technology Centre (ESTEC), 2200 AG Noordwijk, The Netherlands*

a b s t r a c t

The secondary electron emission (SEE) from materials used in high power RF devices in space is the main trigger and sustaining mechanism of the resonant avalanche electron discharge known as the multipactor effect. It limits the attainable power of those devices. During recent decades, some scientific research has been focused on material properties for obtaining anti-multipactor coatings of low secondary emission yield (SEY). The European Space Agency (ESA) is leading a technological research on a new approach based on surface roughness that might perform as a kind of blackbody or Faraday cage effect. A multilayer coating structure was adopted for fulfilling the stringent requirements of the space. The surface of a standard silver plating was modified by a two-step treatment. First, a wet chemically etching process created a roughness of high aspect ratio, in the scale of microns. Secondly, the surface was coated with a protective 2 μ,m overlayer of gold, using magnetron sputtering. This anti-multipactor coating has been tested on several types of K_u-band WR75 waveguide transformers and band-pass filters, with excellent results. The multipactor effect was suppressed for two waveguides, even when applying the maximum available power levels. As for the other final four, the increase of multipactor power level was in the range of 4–6 dB. These results were obtained after more than one year of air exposure. In spite of the strong roughness, the insertion losses were diminished by 25% with respect to the values attained in the tests of the standard anti-multipactor coating, Alodine.

1. **Introduction**

Multipactor (MP) is a complex, potentially detrimental phenomenon targeted for mitigation in the past few decades, with the purpose of increasing the levels of stable delivered power in space missions. Similar phenomena take place in high-energy particle accelerators [1,2], in magnetically confined fusion apparatus [3] and other vacuum high power RF devices, such as klystrons [4]. The dynamic mechanism that defines it is the resonant multiplication of the secondary electron population in RF components, that can eventually lead to: (i) modification of device impedance, (ii) absorption and reflection of RF power, (iii) enhancement of noise, (iv) generation of harmonics, (v) outgassing from exposed surfaces, and finally (vi) destructive corona discharge.

Previous research was carried out to improve the performance of the current anti-multipactor Alodine coating [5–12]. In the traditional approach based on materials properties, metals and metallic compounds with initial low SEY and surface resistance were proved to be unstable in air and affected by aging processes. Since any kind of in situ surface conditioning was completely discounted, a trade off seemed to come from noble, inert metals. As a result, gold coating of a chemically etched silver surface was considered as a viable alternative for several additional reasons:

(a) the surface roughness of silver insures a high first cross-over energy E_1 (the energy at which the SEY is first equal to one) and a low SEY coefficient;
(b) oxidation of silver is prevented with a metal of even higher E_1;
(c) low RF surface resistance is maintained and
(d) the chemical and physical structure is stable to long term air exposure.

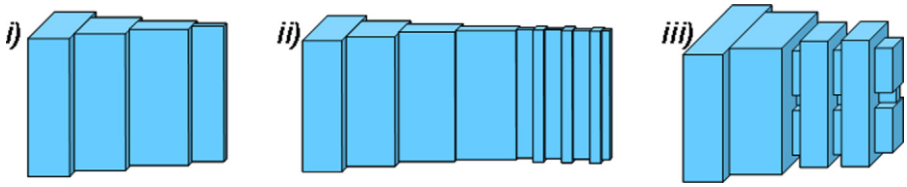

Fig. 1. Schematic diagram for the geometric half - structure of the multipactor samples. (i) reduced height gap transformer, of three types, (ii) corrugated low pass filter, and (iii) ridged low pass filter. Not to scale.

The secondary electron emission from materials used in high power RF devices in space is the main trigger and sustaining mechanism of the resonant avalanche electron discharge known as the multipactor effect [13–16]. It limits the attainable power and the optimum performance of these devices. The multipactor resonance conditions can often be avoided by an appropriate design of the electromagnetic field; even though, there are always some critical parts where a low secondary emission yield is required. For decades, research has focused on material properties to obtain anti-multipactor coatings of low secondary emission yield (SEY). This approach has shown its limitations in space applications where strong requirements on stability in atmospheric air and surface electrical conductivity are set. ESA is leading technological research on a new approach based on surface roughness, which might work as a kind of blackbody or Faraday cage effect [37]. There are several simulation and experimental results [17–19] demonstrating that high aspect ratio surface roughness is capable of absorbing part of the electron emission in the so-called SEY "suppression" effect. This effect is purely macroscopic and independent of roughness size or material type. It is caused by the appropriate roughness profile. Researchers from the particle accelerator scientific community (SLAC, KEKB, CERN) are proposing macroscopic grooved surfaces in specific regions, to avoid the e-cloud build up negative effects [20–22].

We report here the first application of microscopic surface roughness for high power RF devices in space applications.

2. **Experimental**

2.1. *Samples*

Two main kinds of samples were manufactured, treated and tested in this work: small research samples and multipactor samples. Both were made of silver plated aluminum 6061 alloy, as is standard in space industry and manufactured by Tesat Spacecom.

Table 1
Types of multipactor samples of standard silver plating "as received" from Tesat, to be treated in our labs.

Item	Sample	Gap (mm)	Ag thickness (μ,m)
K_u0	Short gap transformer (type 1)	0.14	20
K_u1	Short gap transformer (type 1)	0.14	20
K_u2	Long gap transformer (type 2)	0.14	40
K_u3	Gap transformer (type 3)	0.10	40
K_u4	Gap corrugated low pass filter	0.34	40
K_u5	Gap ridged low pass filter	0.70	40

The small research samples were about (50 mm × 20 mm × 1 mm) with 20 μ,m Ag plating. Smaller research samples about (13 mm × 10 mm × 1 mm) were sectioned from them and used in the research of the appropriate wet chemical etching procedure, for a surface porosity or roughness of high aspect ratio, in the micron size scale.

The multipactor samples were actual RF waveguides (K_u-band, WR75 for 11.8 GHz) specially designed and manufactured by Tesat Spacecom for multipactor and RF performance tests after surface treatment. Their external size was about (40 mm × 20 mm × 110 mm). They were manufactured in three main structures: (i) a waveguide with reduced height gap and transformers on both ends, (ii) a corrugated low pass filter, and (iii) a ridged low pass filter (Fig. 1 shows half of the inner volume). The gap transformers were of three types as shown in Table 1.

The multipactor test samples were comprise of two symmetrical half shells, as shown in Fig. 2, to facilitate the surface treatment and analysis. Five final multipactor samples, Ku1–5 (see Table 1) were tested at Tesat Spacecom for multipactor threshold and RF performance after completing the surface treatment (i.e., with the new rough coating) and another identical five ones without surface treatment (i.e., with standard silver-plating). An initial multipactor

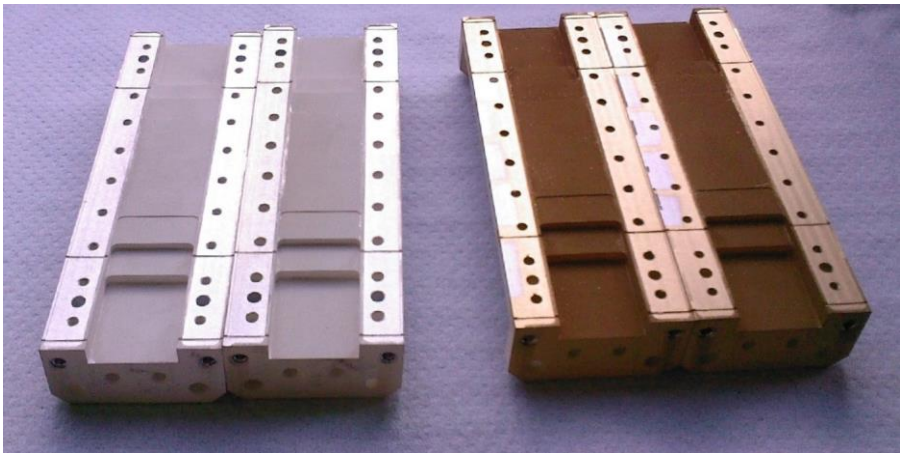

Fig. 2. Multipactor test sample Ku3-left and Ku2-right at the two stages of the surface treatment, shown with the half shell structure open apart. Notice the darker and matte appearance of the roughened Ag and Au surfaces, compared to a standard silver surface.

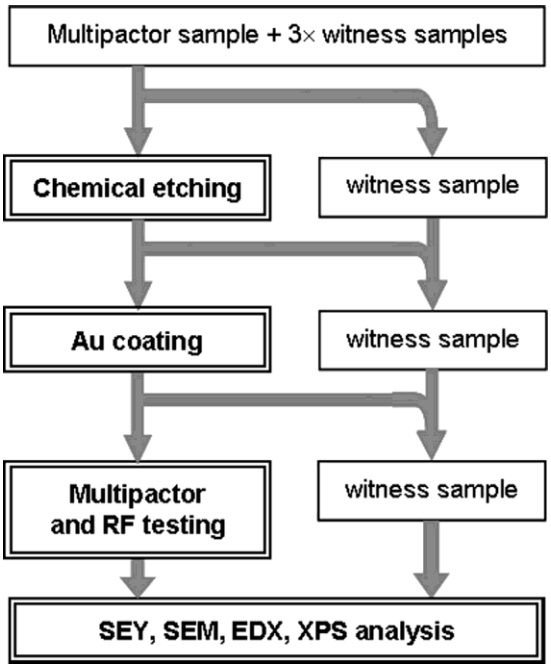

Fig. 3. Schematic diagram of the surface treatment and testing of the multipactor samples. Witness samples were small research samples. Some multipactor large samples also were analyzed by SEY, SEM, EDX and XPS.

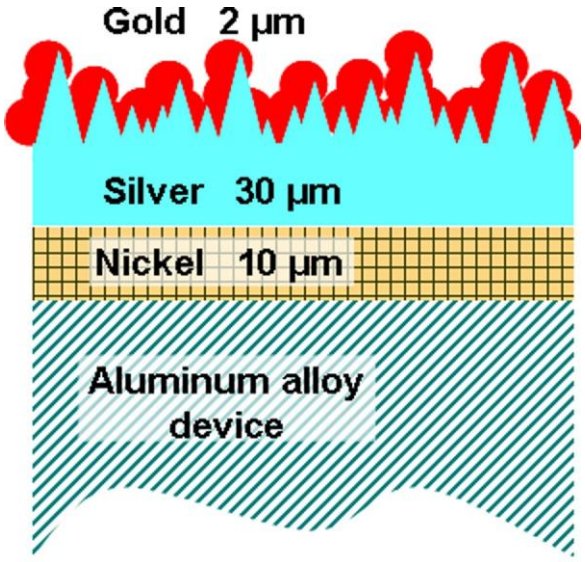

Fig. 4. Schematic diagram of the final multilayer anti-multipactor coating the Au over layer: for low SEY surface, electrical conductivity and chemical stability, the Ag layer: for a high aspect ratio surface roughness and electrical conductivity, the Ni layer: for improved adhesion.

sample, K_{u0} was tested at ESA/ESTEC at the three stages of surface treatment: (a) plain Ag plating before any treatment, (b) chemically etched Ag plating, and (c) after chemically etching and Au coating.

Since surface treatment optimized for small research samples did not work equally well for the larger multipactor test samples, several initially similar multipactor samples have been used for adapting the chemical etching procedure to the larger samples.

2.2. *Surface treatment*

Surface treatment was developed in our laboratories, in two main steps or phases: wet chemical etching of the silver-plating, to achieve the appropriate surface roughness and on-top a gold deposition to obtain an oxidation protective surface overlayer of low SEY. The final optimized procedure for surface treatment of the multipactor samples is schematically described in the diagram of Fig. 3.

During surface treatment, several surface analysis techniques were used: mainly SEY measurements, SEM (Scanning Electron Microscopy), EDX (Energy Dispersive X-ray emission spectroscopy, associated to SEM), and XPS (X-ray Photoemission Spectroscopy). Final multipactor test samples were also analyzed by these techniques. The multilayer structure and functions of the final anti-multipactor coating is summarily described in diagram of Fig. 4.

2.3. *Wet chemical etching of silver*

In the first phase of the surface treatment, a porous surface was chemically etched on the silver plating by an acid mixture. High structuring is necessary for a SEY "suppression effect". However, roughness sizes bellow 10 μ,m were necessary for the geometrical precision, required by the microwave wavelength. This was accomplished by wet chemical etching. It is a well-known procedure, mostly implemented in the fabrication of structured silicon wafers and micro-technology [23–25]. The etchant utilized was adapted for silver in order to meet those requirements. Several common potential etchants were tried under a variety of conditions: (a) $HNO_3 + HF + H_2O$, (b) $CH_3OH + NH_4OH + H_2O_2$, (c) $KI + I_2 + H_2O$, (d) $HCl + HNO_3 + H_2O$, and (e) $H_2SO4 + H_2O_2$. The size of the roughness was analyzed by SEM and the suitable aspect ratio was detected by its "suppression effect" in SEY. This last criterion was much more restrictive that the first one. The common quartz cleaning solution (a) was clearly the preferred choice, with maximum SEY values below 1.5 (values for the as - received Ag plating, 1.8–2.6). It was found that a simple, easy discernable criterion was a darkened matte surface to the naked eye.

We describe here the chemical etching adjusted for the large multipactor test samples. That of the small research samples was not so critical in the conditions. The reproducibility was tested with 40 research samples and 10 multipactor samples. Ag plating thickness of 10, 20, and 40 μ,m were tested; 40 μ,m was necessary to avoid over etching in sharp corners.

Prior to the chemical etching, surface contamination was removed by successive treatments in ultrasonic baths of acetone, methanol and deionised water, respectively, at room temperature during a total of 10 min, and then dried out by nitrogen flow.

A mixture of 500 cm^3 deionised water (18 MΩ), 60 cm^3 of HF 48 wt% PA-ACS-ISO ($M = 20.01$), then 250 cm^3 of HNO_3 65 wt% PRS ($M = 63.01$), and then 190 cm^3 of water to complete a total volume of 1000 cm^3 is prepared in a high-density polyethylene or similar acid resistant container. Since this is an exothermal reaction, an increase of about 10 °C above room temperature is detected, along with gas release at the surface. Then, the solution is poured in a bath, a 2000 cm^3 acid resistant vessel with suitable dimensions for the solution to cover the lying waveguide half shell by 3 cm. Best results are obtained if the solution is allowed to cool down to 28 °C. Once this occurs, one half-shell and its corresponding witness samples are totally immersed at the same time, with the surface to be treated (inner surface of the waveguide) facing upwards. Then, corrosion starts with visible changes in colour shade and brightness of the silver surface during the optimum etching time of about 2 min, 30 s. The process is also accompanied by the formation of very small gas bubbles over the surface. The most probable reactions, which take

place in a cold and diluted mixture, at the unsaturated molar ratio of H_2O:HNO_3:HF = 31.2:1:79.1 are:

$$3Ag + 4HNO_3 \rightarrow 3AgNO_3 + 2H_2O + NO$$

$$4AgNO_3 + 2H_2O \rightarrow 4Ag + 4HNO_3 + O_2$$

$$AgNO_3 + HF \rightarrow AgF + HNO_3$$

$$4HNO_3 \leftrightarrow 2H_2O + 4NO_2 + O_2$$

The process is stopped before the surface exceeds the desired level of structuring, by taking the samples out of the bath and rinsing in abundant deionised water, using ultrasound. This step is important and necessary for washing out rest of etchant and small particles from the etching reaction. Field emission from these loosely attached particles will trigger multipaction, a well-known problem in other technologies [26]. As a final step, the samples are dried with nitrogen flow and stored in UHV conditions. The entire procedure and conditions are repeated for the second half-shell of the waveguide and its corresponding witness samples.

2.4. Gold coating by magnetron sputtering

In the second phase of the surface treatment, the etched surface of the Ag plating was coated by a Au overlayer to avoid oxidation upon exposure to air. This metal has the best electrical conductivity among inert metals and its SEY is lower than that of Ag exposed to air.

After several trials, a 2 μ,m thick coating by magnetron sputtering was selected. The deposition was performed in a UHV system with a RF magnetron IONX of Thin Film Consulting, with a 2 inch Au target as an atomic source and a base pressure below 10^{-7} mb. This setup insures a stable deposition rate in the range of 65–85 nm/min for normal sputtering conditions. The two half shells of a waveguide are located in a rotating sample stage at 7 cm distance and 50° take off angle from the source. Deposition was performed at 6×10^{-3} mb pressure and 17.7 ml_n/min (millilitre normal per minute) flow of Ar and 110 W of RF transmitted power, while the samples are heated at 120 °C both by the magnetron plasma and by several halogen lamps located in the proximity of the sample stage.

2.5. XPS and SEY apparatus

For the SEY measurements, an EQ22/35 Leybold Hereaus electron gun supplied the incident or primary electron beam: current 0.6–6 nA, diameter 6 mm, fluence 20 nC/mm^2. The SEY measurements were performed by measuring sample current to ground I_s, by a precision electrometer (see Fig. 5).

The incident electron gun current I_p was measured both by a Faraday cup and by a graphite reference sample biased to +50 V and corrected for backscattered emission in the case of graphite. Because of charge neutrality in a conductive sample at constant bias, the emission current is: $I_\sigma = I_s - I_p$, and the SEY is: $a = -I_\sigma/I_p = I_\sigma/|I_p| = 1 + (I_s/|I_p|)$. The primary electron energy is $E_p = e \cdot (V_s - V_g)$, where e is the electron charge, V_s the sample bias, and V_g the electron gun cathode potential (the bias $V_s \approx -30$ V was applied to inhibit secondary electrons, produced elsewhere in the apparatus, from impinging on the sample). When biasing a sample to $V_s = +50$ V, the emission current is only that of the backscattered electrons (with energies typically above 50 eV) $I_{11} = -r_i I_p = I_s - I_p - I_\sigma^*$, where r_i is the backscattering electron emission coefficient and I_σ^* is the current of secondary electrons from elsewhere in the apparatus (since now there is no retarding bias of −30 V, but an accelerating one of +50 V). This current I_σ^* is mainly generated by the sample backscattered electrons. In the case of a graphite sample, I_{ri} is small [27], and I_a^* even smaller, thus practically negligible. In this case, the $I_p \approx I_s/(1 - r_i)$. In our system, the

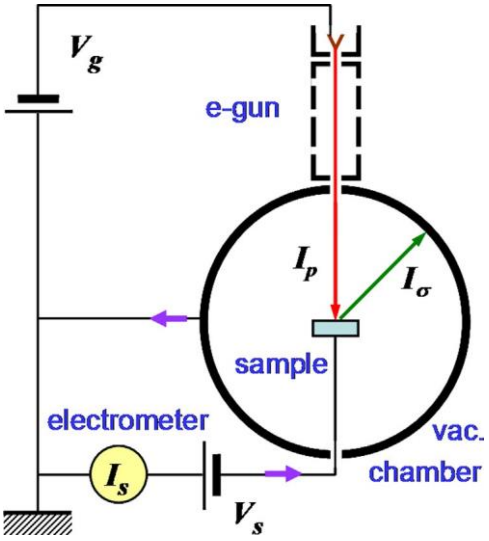

Fig. 5. Schematic diagram of the SEY measurements.
I_p = primary electron beam current, negative. I_σ = emitted secondary electron current, positive. I_s = sample current, the sign of $(a - 1)$ Sample is biased inside the analysis vacuum chamber.

error of this equation is about 3%, similar to that of our Faraday cup method. This error implies a similar error in a. The SEY measurements were performed in a LH10 Leybold Hereaus system under vacuum conditions of 2×10^{-9} mb of base pressure.

In another analysis system (at CSIC–ICMM, Madrid), a Kimball Physics ELG-2 electron gun with fluencies in the fC/mm^2 range was used for tests. This system was capable of measuring SEY of the large multipactor test samples; an ultra-short pulsed electron beam was also available. Additional information can be found in [15].

As for the surface chemical analysis, we made use of an ESCALAB 210 VGS system, equipped with twin anode MgK_U/AlK_U non-monochromatic X-ray source, a spherical sector electron energy analyzer with five channeltrons and three-elements electron lens. The system was operated in the constant analyzer energy mode (CAE), with 50 eV of pass energy and a normal emission angle The sample, a very good conductor, was at the analyzer ground potential and the analyzed energy was calibrated with Au and Ag reference samples. Vacuum in the analysis chamber was below 3×10^{-9} mb.

2.6. Multipactor and RF performance tests

The multipactor threshold and RF performance test setups, as well as the standard procedures and process simulations are fully described elsewhere [7,15].

3. Results and discussion

3.1. Scanning electron microscopy (SEM) analysis

The samples characterized by SEM, (see Fig. 6a and b), presented high aspect ratio surface morphology in the range of microns which performs as a multi-Faraday cage function for the incoming electrons, resulting in a overall electron suppression effect.

Macroscopically, the samples lost their brightness and acquired a darker tone of colour, due to the enhanced absorption of the electromagnetic radiation by the curved surface. A sponge-like pattern of sharp points and edges was generated by the chemical etch. The tips were rounded and converted to lose grains slightly packed after the gold coating. Monte Carlo numerical simulations were performed in the past, especially by the particle accelerator scientific community, in order to predict the degree of secondary electron

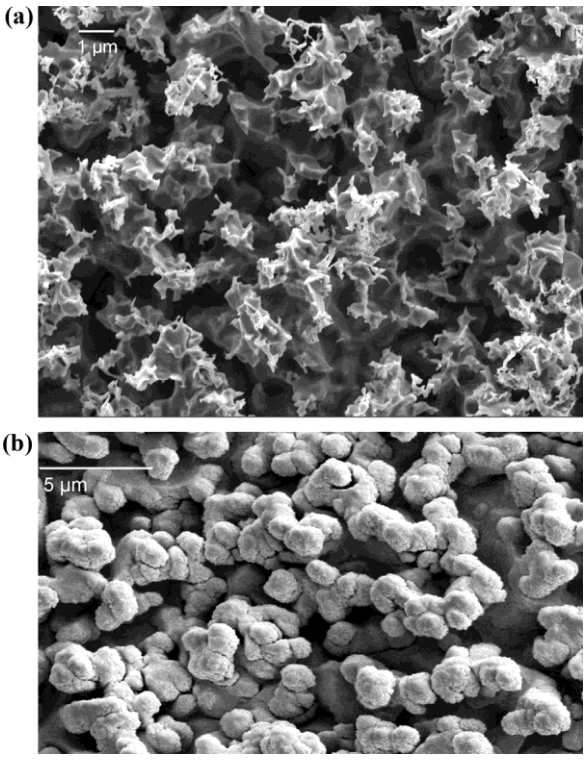

Fig. 6. SEM images of the effect of gold coating a chemically-etched silver sample: (a) silver surface etched by HF-HNO_3, (b) same sample after gold coating by magnetron sputtering.

suppression by rough surfaces. Most of them rely on bidimensional models of triangular or rectangular grooves [17], and on more complex 3D structures, such as a cylindrical well geometry [18]. In all scenarios, the key parameter influencing SEY was the aspect ratio, generally defined as the ratio between the average height and width of every individual cell-unit structure. In addition, the experimental results confirm the SEE (secondary electron emission) suppression effect of high structuring as independent from the roughness size.

Although our real rough surfaces shown in Fig. 6 and Fig. 12 present an important degree of randomness, it was possible to estimate an approximate average protuberance surface density of 0.137 μ,m^{-2} and an approximate 4 μ,m height.

3.2. *XPS and EDX surface composition analysis*

The surface composition and contamination of the silver plating was analyzed by EDX and XPS at two depth scales, 1 μ,m and 5 nm scales, respectively, at two stages: as received and after chemical etching. From the XPS intensities of the Ag 3d, C 1s, O 1s, and F 1s core levels and the corresponding XPS atomic sensitivity factors [28], the near surface composition was calculated and illustrated in Fig. 7.

This is the average composition in a depth of the order of about three photoelectron escape depths, i.e., 9 nm. In addition, no Ag oxide or salt could be detected in the Auger MNN transition (it is not detectable in the 3d core level) [29]; this sets a limit to the amount of surface oxide, below 10%. Thus, it can be concluded that the surface of the silver plating was very similar for both states: a carbonaceous surface overlayer typical of the exposure to air and a silver bulk. The only minor modifications due to the chemical etching process were a small increase (20%) of the contamination carbonaceous layer, a smaller (20%) oxygen composition of this overlayer, and a very small F contamination. The thickness of the carbonaceous surface layer could be estimated from quantitative XPS, if the C atomic density in the overlayer is determined. The relevant equation [30,31] of quantitative XPS is:

$$\frac{I_C}{I_{Ag}} = \frac{S_C \; N_C \; 1-\exp(-d/A)}{S_{Ag} \; N_{Ag} \quad \exp(-d/A)}$$

where I is the XPS intensity, S is the XPS sensitivity factor, N is the atomic density, A is the inelastic mean free path of the photoelectron (≈2.9 nm, for C 1s and Ag 3d photoelectrons in the overlayer), and d the thickness of the overlayer. For computing d, we needed a model compound of well-known specific values for the necessary data. Assuming a $C_5O_2H_8$ initial composition as the closest model, the calculated thickness would be in the range of 6–7 nm for both states.

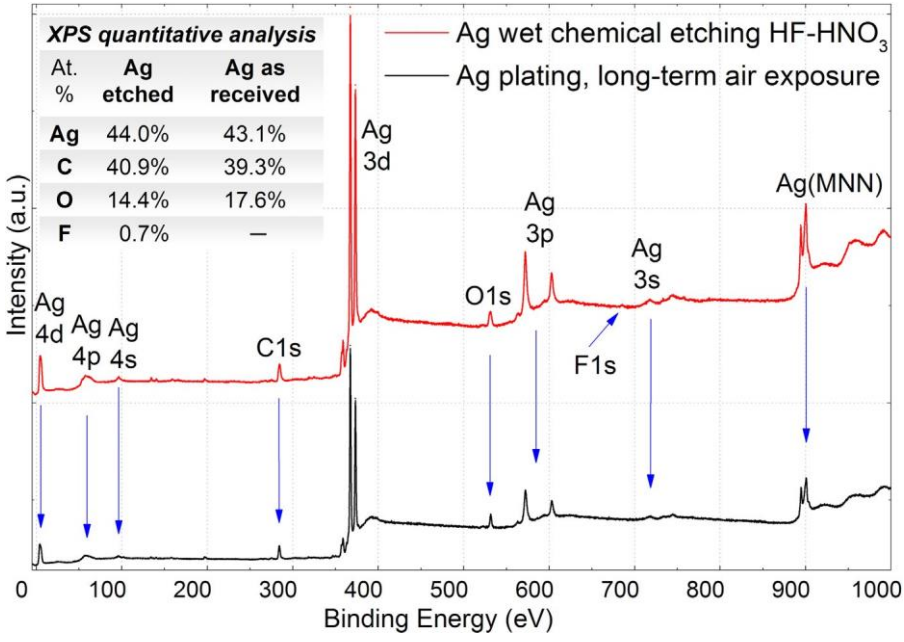

Fig. 7. Surface XPS (MgKu) quantitative analysis of the as-received silver plating,with a long-term exposure to air and the chemically treated by HF-HNO_3 silver research samples.

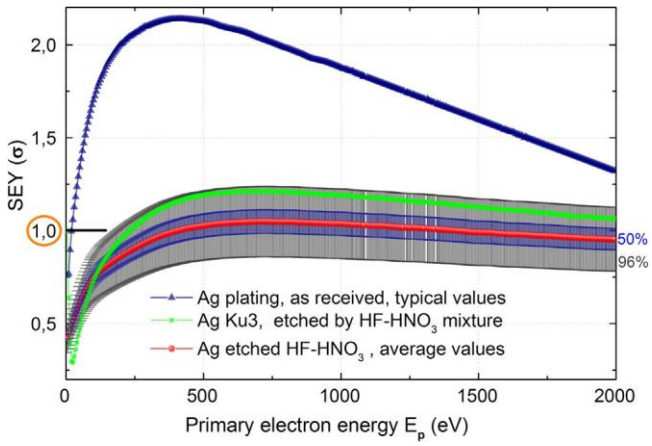

Fig. 8. Comparison between high SEY coefficient of the "as received", smooth plated silver and the average values of wet chemically etched research samples.

Other EDX measurements, using an Oxford Instruments analyzer (model INCAx - sight), were also performed to determine bulk composition. We estimated that an approximate layer of 8 μm in depth of silver was totally removed during the etching process, justifying thus the need for consistent initial plating. After the second step, we determined that the gold signal detected by EDX was 100% on the top of the protuberances. It was not the case for the base region of the grain structure, since shadowing effects affected the uniform coverage. The atomic ratio in bulk detected there (Ag L/Au M) = (12%/88%), suggests that in these lower regions, the average gold layer thickness was well under 2 μm.

3.3. SEY measurements

In Figs. 8 and 9, we present the SEY–energy dependence curves of relevant samples and surfaces in this study. In Fig. 8, the strong SEY suppression effect caused by the surface roughness on Ag plating can be observed. A typical SEY curve of as-received conditions is compared with SEY of chemically etched Ag surfaces. The statistical results of 60 research samples are shown as the average values and the error bars corresponding to 50 and 96% of the samples (computed from the typical deviation values). In this figure, the SEY curve of a typical multipactor sample with a chemically etched silver surface is also depicted. It can be observed that the effect of the chemical treatment is not as effective as on the smaller research samples. Comparing our experimental SEY curves with those from theoretical simulations for different aspect ratios [17,18], we would expect an aspect ratio higher than 2.

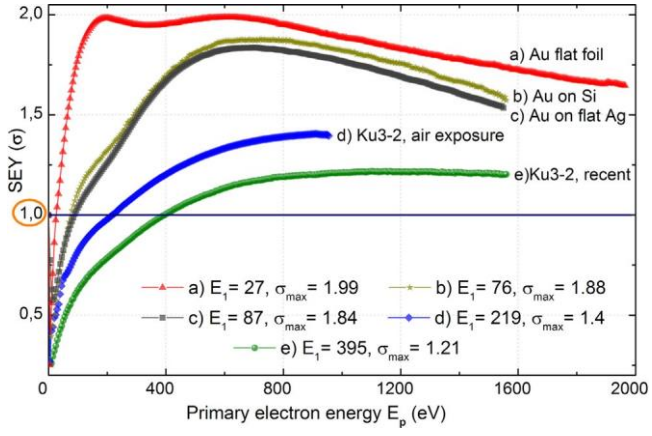

Fig. 9. SEY of relevant Au surfaces: (a) 25 μm Au foil (99.9% pure from Goodfellow), long-term air exposure, (b) 2 μm Au on polished Si wafer, short air exposure. (c) 2 μm Au on Ag plating, short air exposure. (d) 2 μm Au on chemically etched Ag plating, K_u3 multipactor sample, long air exposure (400 day). (e) 2 μm Au on chemically etched Ag plating, K_u3 multipactor sample, short air exposure. All the 2 μm Au coatings were deposited at the same batch.

We should draw attention to the fact that the SEY suppression effect is more pronounced at low primary energies (or vice versa) than is predicted by simulations. This is precisely the best behaviour for anti-multipactor coatings.

Similar effects of surface roughness on the final treated coatings, i.e., with a rough gold surface, are shown in Fig. 9. Rough (e) and smooth (b, c) Au surfaces with short air exposures can be compared, and analogously, for long air exposures (d vs. a). Also, the absence of effect of the substrate material can be observed.

The "shoulder" at low energies (100–200 eV) in the SEY coefficient of Au is due to the adventitious surface carbonaceous contamination "naturally" grown during exposure to air, and well known in XPS practice where it was used for energy referencing [32,33]; at these energies, the primary electron range is of 1–2 nm [34]. This layer is mainly formed by hydrocarbons. Its intensity is related to its thickness [35,36], i.e., to the exposure time. For higher primary energy, the electron range reaches into the Au substrate and its SEY is recovered. The electron range in Ag and Au at 2000 eV is about 50 nm [34], and thus much smaller than the Au layer thickness and the surface roughness size for all energies of interest.

3.4. Multipactor threshold

We present in Table 2 the results of the multipactor threshold tests. These multipactor and SEY tests were performed after very long exposures to the air (more than one year for K_u 1–2). The complete surface treatment, i.e., chemical etching plus the Au coating, produces an increase in the multipactor power level of 2–6 dB with respect to the bare Ag plating in four samples and practical suppression in two samples. For the latter case, it was not possible to initiate the multipactor discharge, even using the maximum available power (6500 W at Tesat and 5300 W at the ESA/ESTEC test centre, respectively). That meant an improvement of >12.7 dB and >8.79, respectively, versus the bare silver plating. This demonstrates that in practice it is possible to avoid multipaction by surface roughness of high aspect ratio. Another important fact to point out is that it is not necessary that SEY < 1, but the first cross-over energy E_1 should be sufficiently high. For the multipactor effect, the important SEY values are those for low primary energies.

In principle, a difficulty in analyzing the multipactor data of Table 2 is that multipactor samples are of different types and different gap heights.Moreover, the low pass filters are not even comparable to parallel plates. Thus, it is no surprise that there is no correlation among frequency-gap product values and multipactor levels. In addition, the influence of SEY parameters on multipactor level could be obscured by the diversity in waveguide structure. Despite all that, there is an evident and strong correlation for the latter. There is a linear correlation between first cross-over energy E_1 and multipactor level. This correlation improves significantly if SEY properties are condensed in the ratio of the first cross-over energy to the SEY maximum ratio E_1/α_m, see Fig. 10. It was even possible to distinguish between the Ag plating and the treated surface (rough Au) behaviour with 1.3% of error.

$$\mathrm{MP(rough\_Au)} = 53\,\mathrm{W}\left(\frac{E_1/1\,\mathrm{eV}}{\alpha_m}\right)^{0,8}$$

For Ag plating, the pre-factor is 108 W, with a 2% error, and the exponent 0.69. If all surfaces are considered, the pre-factor is 120 W and the exponent 0.64, with a corresponding 3% error.

Table 2
Results of the tests on the multipactor (MP) samples.

Multipactor test sample		SEY tests at CSIC		12 GHz RF tests at Tesat		
Sample	Surface	E_1 [eV]	a_m	MP power (W)	MP power increase (dB)	Insertion losses (dB)
K_u0–1	Ag plating	32	2.2	700*		0.15*
K_u0–2	Rough Ag	150	1.3	1100*	1.96*	0.36*
K_u0–3	Rough Au	300	1.3	>5300*	>8.79*	0.52*
K_u1–1	Ag plating	18	2.02	496		0.215
K_u1–2	Rough Au	73	1.51	1172	3.73	0.630
K_u2–1	Ag plating	32	1.83	759		0.281
K_u2–2	Rough Au	166	1.44	2469	5.12	0.786
K_u3–1	Ag plating	29	1.83	350		0.359
K_u3–2	Rough Au	219	1.40	>6500	>12.68	1.067
K_u4–1	Ag plating	37	1.81	945		0.178
K_u4–2	Rough Au	237	1.30	3353	5.5	0.422
K_u5–1	Ag plating	65	1.69	1300		0.065
K_u5–2	Rough Au	269	1.20	3960	4.83	0.137

Rough Ag = chemically etched Ag plating, Rough Au = Au coated rough Ag. *RF tests at ESA/ESTEC; >, no multipactor, tested up to the limit of delivered RF power.

3.5. *RF performance*

The RF performance parameter of the multipactor samples relevant for analyzing the surface treatment is the Insertion Loss (IL), of which values are presented in Table 2. In a metallic waveguide, IL in dB is proportional to the surface resistance for a given geometry and frequency. Since multipactor samples were coated roughly uniformly over their entire surface, we may compare pairs of IL values for each waveguide structure as a measurement of the relative surface resistance. Thus, it is computed an increase of 2.8 ± 0.4 in surface resistance for the rough Au surfaces respect to the Ag plating; this is due to surface roughness and higher resistivity. From previous studies with Alodine coating (reference anti-multipactor coating for ESA) in C- and X-band waveguides [37], an increase of 3.8 ± 0.5 should be expected for Alodine coating in the case of the K_u-band multipactor samples of this work. Since the RF field skin depth in the Au coating (0.69 μ,m) is smaller than its thickness and since surface resistance is proportional to the square root of the bulk dc resistivity (1.59 and 2.44 μ,Ωcm for Ag and Au, respectively), we may separate the effect of the material and the effect of the roughness. Thus, it is computed an increase of 2.3 ± 0.3 in surface resistance for the rough Ag surfaces respect to the Ag plating, i.e., due only to surface roughness. In this case, we are disregarding the modification of surface roughness by the Au coating, as confirmed by K_u 0–2.

We have compared these results with theoretical calculations for the influence of surface roughness on RF surface resistance.

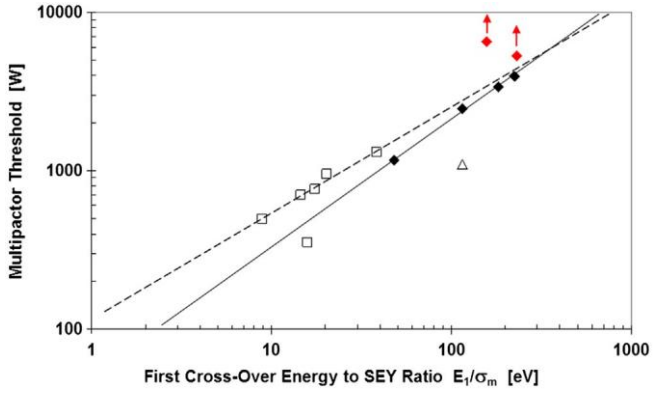

Fig. 10. Correlation between multipactor power level and the SEY parameters of this coating. Squares: Ag plating, Triangle: chemically etched Ag, Diamonds: Au coated chemically etched Ag. Multipactor suppression for diamonds marked by an arrow (maximum tested power) is shown.

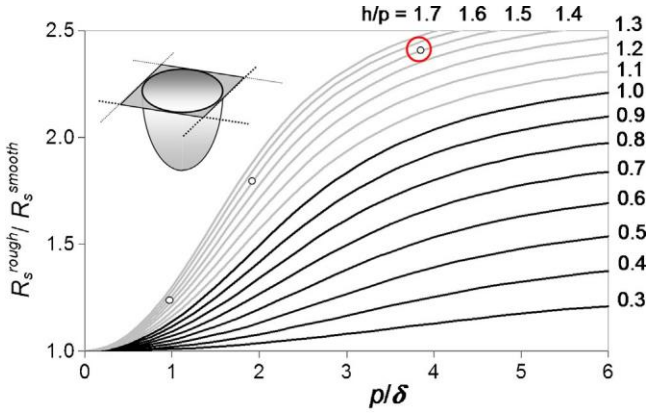

Fig. 11. Roughness factor in surface resistance for semi-ellipsoidal indentations of radius and period p and height h. Black curves ($h/p \le 1$), theoretical data from [28]; grey curves, approximate extrapolations; ι, skin depth. The highlighted dot corresponds to $p = 2.7$ μ,m, $h/p = 1.5$, $\iota = 0.7$ μ,m.

These theoretical predictions [38,39] were made for simple, regular geometrical profiles. As an approximate model to our experimental irregular and partly random surface roughness, we chose the tangent semi-ellipsoidal indentations, distributed with square translation symmetry, which leave protuberances in the square corners (Fig. 11). The corresponding RF surface resistance has been numerically computed in [39].

We used the surface roughness parameters: protuberance surface density and height, estimated from SEM images of Fig. 6b and Fig. 12, for computing Fig. 11 using data from [39], which shows a

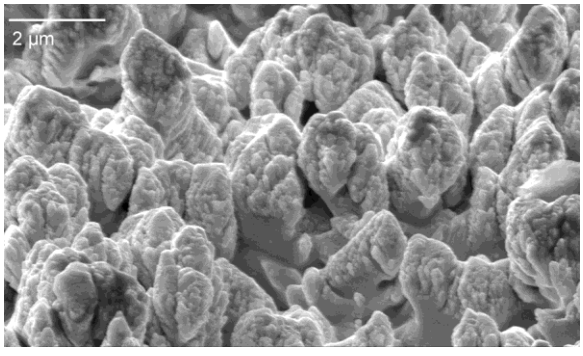

Fig. 12. Cross section of the K_u3–2 surface morphology, for the estimation of roughness parameters. SEM image in angle perspective of about 15° take-off angle.

surface resistance roughness factor of 2.4 in excellent agreement with our experimental results of RF insertion loss.

4. Summary and conclusions

A research on anti-multipactor coatings based on surface roughness has been undertaken, since the approach based on material properties has reached a limit due to the problem of aging in atmospheric air, unavoidable in space applications. A multilayer coating structure has been adopted for the fulfilment of these requirements. The standard conductive layer of Ag plating is preserved but its surface is modified by a two-step treatment. First, a high aspect ratio roughness on the scale of microns is chemically etched. Secondly, it is further coated by 2 μm of gold. This multilayer anti-multipactor coating has been tested on K_u-band WR75 waveguides of several types, with excellent results. Multipactor has been suppressed for two of them, reaching even the maximum available power level (equivalent of >12 dB over the standard Ag plating). For the other four waveguides, the increase of multipactor power level was of 4–6 dB. These results were obtained after more than one year of air exposure, which should be attributed to the gold protective overlayer.

In spite of the strong roughness, the insertion loss was increased in a factor of 2.8 ± 0.4 compared to a factor of 3.8 ± 0.5 expected for Alodine, the reference anti-multipactor coating for ESA. The insertion loss will be further diminished in future work by decreasing the roughness size scale and experimental results are planned for publishing.

The wet chemical etching of Ag plus sonication in deionised water leaves a highly porous or sponge-like chaotic surface roughness without any extra contamination apart from that due to air exposure. The 2 μm Au coating results in a distribution of protuberances ranging 1–5 μm in height and 1–2 μm in width.

The effect of suppression of the secondary electron emission by the surface roughness of high aspect ratio was much more pronounced at low primary energies than predicted by published simulation model results. This is just the desired effect for an anti-multipactor coating. The main SEY requirement is a high first cross-over energy. We still need to determine in what manner the backscattered and true secondary electrons trigger and sustain the electronic suppression effect.

Recent studies on antimultipactor structures of tens of nanometres are intended for future publication.

Acknowledgments

We would like to thank Prof. L. Soriano of the Applied Physics Department (Universidad Autónoma de Madrid), for his collaboration in the preparation of the research samples.

This work was supported by the European Space Agency (ESA)/European Space Research and Technology Centre (ESTEC), under the research program "Porous Inert Metal Coatings for Controlling Secondary Electron Emission", ESA 17025/03/NL/EC (CCN-02) and by the Ministry of Economy and Competitiveness of Spain, the National Plan of R&D&I, coordinated Projects no. AYA2012-39832-C02-01 and -02.

References

[1] Roberto Cimino, Giovanni Rumolo, Frank Zimmermann, Proceedings of ECLOUD'12: Joint INFN-CERN-EuCARD-AccNet Workshop on Electron-Cloud Effects, La Biodola, Isola d'Elba, Italy, 5–9 June, 2012 arXiv:1403.3292.

[2] P. Chiggiato, et al. Thin Film Coatings for Suppressing Electron Multipacting in Particle Accelerators, Conf. Proc. C110328 (2011) 2096-2098 PAC-2011-THOBS6.

[3] Kishore Mishra, et al., Conditioning technique for high power RF vacuum transmission line components using multipactor plasma, J. Phys. Conf. Ser. 208 (012017) (2010).

[4] C. Hill, R.G. Carter, Investigation of Possible Multipactor Discharge in a Klystron Input Cavity, Vacuum Electronics Conf., 2006 held Jointly with 2006 IEEE International Vacuum Electron Sources, IEEE Intl, vol. no., pp. 81, 82.

[5] L. Galán, C. Morant, F. Rueda, J.M. Sanz, J. Barbero, Study of secondary emission properties of materials used for high power RF components in space, Final Report, ESA-ESTEC Contract 6577/85/NL/PB, ESA (1987).

[6] L. Galán, P. Prieto, C. Morant, L. Soriano, F. Rueda, Study of secondary emission properties of materials for high RF power in space, Final Report, ESA-ESTEC Contract 6577/85/NL/PB, ESA (1990).

[7] N. Díaz, S. Castañeda, I. Montero, L. Galán, F. Rueda, Coatings to prevent multipactor effect in RF high power components for space, Final Report, ESA-ESTEC Contract P.O. 162594 (1996), ESA (1998).

[8] N. Diaz, et al. In Workshop on Multipactor, RF and DC Corona and Passive Intermodulation in Space RF Hardware, Sept. 2000, WPP-178, ESA Publications Division (2001).

[9] D. Wolk. et al. AO-4025 ITT ESA–Surface Treatment and Coating for the Reduction of Multipactor and Passive Intermodulation (PIM) Effects in RF Components, MULCOPIM, Workshop, Sept. 2003, ESA Publications Division, ESA (2004).

[10] A. Ruiz, E. Román, P. Lozano, M. García, I. Montero, L. Galán, D. Wolk, D. Raboso, Ti, V, and Cr Nitride Coatings for Reduction of Multipactor Effects in RF Components, in 5th Int. Workshop on Multipactor, Corona and Passive Intermodulation in Space Hardware (MULCOPIM), Sep 2005, ESA Publications Division. c/o ESTEC PO Box 299 AG Noordwijk, Netherlands.

[11] D. Wolk, P. Lozano, M. García, I. Montero, L. Galán, C. Prieto, F. Galán-Estella, E. García-Camarero, D. Raboso, Coatings on Mg Alloys for Reduction of Multipactor Effects in RF Components, in 5th Int. Workshop on Multipactor, Corona and Passive Intermodulation in Space Hardware (MULCOPIM), Sep 2005, ESA Publications Division. c/o ESTEC PO Box 299 AG Noordwijk, Netherlands.

[12] L. Galán, M. García, P. Lozano, I. Montero, E. Román, Multipaction study and coating selection. In Surface Treatment and Coating for the Reduction of Multipactor and Passive Intermodulation (PIM) Effects in RF Components, Final Report ESA/ESTEC Contract No. 17025/03/NL/EC, ESA/ESTEC.

[13] A. Woode, J. Petit, Diagnostic investigations into the multipactor effect, susceptibility zone measurements and parameters affecting a discharge, ESTEC Working Paper No. 1556, ESTEC ESA (Nov. 1989).

[14] R.A. Kishek, Multipactor discharge on metals and dielectrics: Historical review and recent theories, Physics of Plasmas, Vol. 5, No. 5, May 1998.

[15] European Cooperation for Space Standardization, Space Engineering, Multipaction Design and Tests, ECSS-E-20-01A Rev.1, March 2013.

[16] Anza Sergio, et al. Prediction of Multipactor Breakdown for Multicarrier Applications: The Quasi-Stationary Method. Microwave Theory and Techniques, IEEE Transactions on 60.7 (2012) 2093–2105.

[17] M. Pivi, F.K. King, R.E. Kirby, T.O. Raubenheimer, G. Stupakov, F. Le Pimpec, Sharp reduction of the secondary electron emission yield from grooved surfaces, J. Appl. Phys. 104 (2008) 104904–104910.

[18] M. Ye, Y.N. He, S.G. Hu, R. Wang, T.C. Hu, J. Yang, W.Z. Cui, Suppression of secondary electron yield by micro-porous array structure, J. Appl. Phys. 113 (074904) (2013).

[19] S.W. Lee, Y.J. Baik, C.J. Kang, D. Jeon, Suppression of secondary electrons from diamond by whisker formation, Appl. Surf. Sci. 215 (2003) 265–268.

[20] A.A. Krasnov, Vacuum 73 (2004) 195.

[21] M. Venturini, M., Furman, J.-L. Vay, M. Pivi, Modelling of e-cloud build-up in grooved vacuum chambers using POSINST, Proceedings of PAC07, Albuquerque, New Mexico, USA.

[22] Y. Suetsugu, H. Fukuma, K. Shibata, M. Pivi, L. Wang, Experimental studies on grooved surfaces to suppress secondary electron emission, Proceedings of IPAC'10, Kyoto, Japan.

[23] C. Benoit-Moez, S., Bastide, C. Lévy-Clément, Silicon Nanowires: Condition of Synthesis and Size Selection, 23rd European Photovoltaic Solar Energy Conference and Exhibition, Sept. 2008, Valencia, Spain, pp. 641–644.

[24] M. Steinert, J. Acker, M. Krause, S. Oswald, K. Wetzig, Reactive species generated during wet chemical etching of silicon in HF/HNO3 mixtures, J. Phys. Chem. B 110 (2006) 11377–11382.

[25] Kurt W. Kolasinski, Silicon nanostructures from electroless electrochemical etching, Current Opinion in Solid State and Materials Science, Volume 9, Issues 1–2, February–April 2005, pp. 73–83, ISSN 1359-0286.

[26] H. Padamsee, J. Knobloch, The Nature of Field Emission From Microparticles and the Ensuing Voltage Breakdown, SRF 981021-14, RF' 98 conf., 1998.

[27] J. Cazaux, Electron back-scattering coefficient below 5 keV: Analytical expressions and surface-barrier effects, J. Appl. Phys. 112, 084905 (2012).

[28] C.D. Wagner, D. Briggs, M.P. Seah, Practical Surface Analysis, Vol. 1., 2nd Edition, published by J. Wiley and Sons, 1990, ISBN 0-471-92081-9.

[29] A.M. Ferraria, A.P. Carapeto, A.M. Botelho do Rego, X-ray photoelectron spectroscopy: silver salts revisited, Vacuum 86 12 (2012) 1988–1991.

[30] M.P. Seah, Quantification in AES and XPS, in Surface Analysis by Auger and X-ray Photoelectron Spectroscopy, in: D. Briggs, J.T. Grant (ed.), IM Publication and Surface Spectra, 2003, p. 345.

[31] D.Y. Petrovykh, J.M. Sullivan, L.J. Whitman, Quantification of discrete oxide and sulfur layers on sulfur-passivated InAs by XPS, Surf. Interface Anal. 37 (2005) 989–997.

[32] R.E. Davies, J.R. Dennison, Evolution of secondary electron emission characteristics of spacecraft surfaces, J. Spacecraft Rockets 3 (4) (1997) 571–574.

[33] T.L. Barr, S. Seal, Nature of the Use of Adventitious Carbon as a Binding Energy Standard, J. Vacuum Sci. Technol., 13 (3 (pt. 2)) (1995) 1239–1246, May/June.
[34] G. Wilson, J.R. Dennison, Approximation of range in materials as a function of incident electron energy, IEEE Trans. Plasma Sci. 40 (2) (Feb 2012) 291–297.
[35] J.R. Dennison, Ryan Hoffmann, Effects on Spacecraft Charging of Modification of Materials by Space Interactions Environment, 11th Spacecraft Charging Conference, Albuquerque New Mexico, September 20–25, 2010.
[36] SeGi Yu, Whikun Yi, Taewon Jeong, Jeonghee Lee, Jungna Heo, Chang Soo Lee, D. Jeon, J.M. Kimb, Secondary electron emission for layered structures, J. Vac. Sci. Technol. A 20 (3), May/June 2002.
[37] Surface treatment and coating for the reduction of Multipactor and PIM effects in RF components. ESA–TesatSpacecom contract no. 17025/03/NL/EC. ESA, Noordwijk, Netherlands.
[38] A. Matsushima, K. Nakata, Power loss and local surface impedance associated with conducting rough interfaces, Elect. Commun. Jpn., 89 (1 (pt. 2)) (January 2006) 1–10.
[39] M.V. Lukic, D.S. Filipovic, Modeling of 3-d surface roughness effects with application to μ,-coaxial lines, IEEE Trans. Microwave Theory Techn. 55 (2007) 518–525.